This article is a *Plant Cell* Advance Online Publication. The date of its first appearance online is the official date of publication. The article has been edited and the authors have corrected proofs, but minor changes could be made before the final version is published. Posting this version online reduces the time to publication by several weeks.

Arabidopsis Annexin1 Mediates the Radical-Activated Plasma Membrane Ca^{2+}- and K^+-Permeable Conductance in Root Cells[W]

Anuphon Laohavisit,[a,1] Zhonglin Shang,[a,1,2] Lourdes Rubio,[a,3] Tracey A. Cuin,[b,4] Anne-Aliénor Véry,[c] Aihua Wang,[d] Jennifer C. Mortimer,[a,5] Neil Macpherson,[a,6] Katy M. Coxon,[a,7] Nicholas H. Battey,[e] Colin Brownlee,[f] Ohkmae K. Park,[g] Hervé Sentenac,[c] Sergey Shabala,[b] Alex A.R. Webb,[a] and Julia M. Davies[a,8]

[a] Department of Plant Sciences, University of Cambridge, Cambridge CB2 3EA, United Kingdom
[b] School of Agricultural Sciences, University of Tasmania, Hobart, Tasmania 7001, Australia
[c] Biochimie et Physiologie Moléculaire des Plantes, Unité Mixte de Recherche 5004 Centre National de la Recherche Scientifique/Institut National de la Recherche Agronomique/SupAgro-M/UM2, 34060 Montpellier cedex 2, France
[d] College of Life Science, Hebei Normal University, Shijiazhang 050016, Hebei, China
[e] School of Biological Sciences, University of Reading, Whiteknights, Reading RG6 6AS, United Kingdom
[f] Marine Biological Association, Plymouth PL1 2PB, United Kingdom
[g] School of Life Sciences and Biotechnology, Korea University, Seoul 136-701, Korea

Plant cell growth and stress signaling require Ca^{2+} influx through plasma membrane transport proteins that are regulated by reactive oxygen species. In root cell growth, adaptation to salinity stress, and stomatal closure, such proteins operate downstream of the plasma membrane NADPH oxidases that produce extracellular superoxide anion, a reactive oxygen species that is readily converted to extracellular hydrogen peroxide and hydroxyl radicals, $OH^{\bullet}$. In root cells, extracellular $OH^{\bullet}$ activates a plasma membrane Ca^{2+}-permeable conductance that permits Ca^{2+} influx. In *Arabidopsis thaliana*, distribution of this conductance resembles that of annexin1 (ANN1). Annexins are membrane binding proteins that can form Ca^{2+}-permeable conductances in vitro. Here, the *Arabidopsis* loss-of-function mutant for annexin1 (*Atann1*) was found to lack the root hair and epidermal $OH^{\bullet}$-activated Ca^{2+}- and K^+-permeable conductance. This manifests in both impaired root cell growth and ability to elevate root cell cytosolic free Ca^{2+} in response to $OH^{\bullet}$. An $OH^{\bullet}$-activated Ca^{2+} conductance is reconstituted by recombinant ANN1 in planar lipid bilayers. ANN1 therefore presents as a novel Ca^{2+}-permeable transporter providing a molecular link between reactive oxygen species and cytosolic Ca^{2+} in plants.

INTRODUCTION

Plant cells use cytosolic free Ca^{2+} ($[Ca^{2+}]_{cyt}$) in signal transduction and growth, yet the molecular identities of the Ca^{2+}-permeable transporters that permit Ca^{2+} influx remain largely undiscovered (reviewed in Dodd et al., 2010). Two Pore Channel1 releases vacuolar Ca^{2+} in *Arabidopsis thaliana* (Dodd et al., 2010). The Cyclic Nucleotide-Gated Channel (CNGC) family is implicated, with CNGC2 forming a plasma membrane (PM) Ca^{2+}-permeable channel in *Arabidopsis* for defense and senescence (Dodd et al., 2010; Ma et al., 2010). *Arabidopsis* loss-of-function mutants implicate glutamate receptor–like channels in stress signaling and pollen tube growth (Qi et al., 2006; Dodd et al., 2010; Michard et al., 2011). As yet, the genetic identities of the PM Ca^{2+} influx transporters that are regulated by reactive oxygen species (ROS) to elevate $[Ca^{2+}]_{cyt}$ are unknown. In root cell growth, adaptation to salinity stress, and stomatal closure, these operate downstream of the PM NADPH oxidases that produce extracellular superoxide anion, a ROS readily converted to extracellular hydrogen peroxide and hydroxyl radicals, $OH^{\bullet}$ (Demidchik et al., 2003, 2010; Foreman et al., 2003; Kwak et al., 2003; Chung et al., 2008; Dodd et al., 2010; Laohavisit et al., 2010). In plants, extracellular $OH^{\bullet}$ are thought to coordinate growth and stress responses (Foreman et al., 2003; Renew et al., 2005; Müller et al., 2009; Demidchik et al., 2010). The *Arabidopsis* root epidermal PM contains a Ca^{2+}-permeable conductance (activated by

[1] These authors contributed equally to this work.
[2] Current address: College of Life Science, Hebei Normal University, Shijiazhang 050016, Hebei, China.
[3] Current address: Departamento de Biología Vegetal, Facultad de Ciencias, Universidad de Málaga, Campus de Teatinos, 29071 Malaga, Spain.
[4] Current address: Biochimie et Physiologie Moléculaire des Plantes, Unité Mixte de Recherche 5004 Centre National de la Recherche Scientifique/Institut National de la Recherche Agronomique/SupAgro-M/UM2, 34060 Montpellier cedex 2, France.
[5] Current address: Department of Biochemistry, Hopkins Building, University of Cambridge, Cambridge CB2 1QW, United Kingdom.
[6] Current address: Department of Cell and Systems Biology, University of Toronto, Toronto, Ontario M5S 3G5, Canada.
[7] Current address: Cancer Research UK, Angel Building, 407 St. John St., London EC1V 4AD, United Kingdom.
[8] Address correspondence to jmd32@cam.ac.uk.
The author responsible for distribution of materials integral to the findings presented in this article in accordance with the policy described in the Instructions for Authors (www.plantcell.org) is: Julia M. Davies (jmd32@cam.ac.uk).
[W] Online version contains Web-only data.
www.plantcell.org/cgi/doi/10.1105/tpc.112.097881

extracellular $OH^{\bullet}$), operating in cell elongation and implicated in sodicity stress signaling (Demidchik et al., 2003; Foreman et al., 2003; Chung et al., 2008). In elongation, the conductance lies downstream of the Respiratory Burst Oxidase Homolog C (RBOHC) NADPH oxidase (Foreman et al., 2003) that is the initial source of ROS. The conductance resembles that formed by purified maize (*Zea mays*) annexins incorporated into artificial bilayers containing a lipid peroxidation product (Laohavisit et al., 2010). Hence, an *Arabidopsis* annexin could be responsible for forming the PM $OH^{\bullet}$-activated Ca^{2+} conductance.

Annexins are membrane binding proteins found in pro- and eukaryotes (Morgan et al., 2006). Several animal annexins have been reported to function in vitro as Ca^{2+} channels, including vertebrate annexins A1, 2, 5 to 7, and 12 (Burger et al., 1994; Liemann et al., 1996; Kourie and Wood, 2000). Loss-of-function mutants may have impaired ability to regulate $[Ca^{2+}]_{cyt}$, for example, A5 (−/−) chicken DT40 cells (Kubista et al., 1999), A7 (+/−) murine brain cells (Watson et al., 2004), and A7 (−/−) murine cardiomyocytes (Schrickel et al., 2007). Annexin A5 binds to peroxidized membranes (Balasubramanian et al., 2001) and contributes to peroxide-induced Ca^{2+} influx in chicken DT40 cells (Kubista et al., 1999). However, no studies have causally linked in vitro annexin transport activity to that in native membrane (Konopka-Postupolska et al., 2011). Annexins are abundant throughout the plant kingdom (reviewed in Laohavisit and Davies, 2011a), and some contain the charged residues found in the hydrophobic pore of channel-forming animal annexins (Kourie and Wood, 2000; Laohavisit et al., 2009; Laohavisit and Davies, 2011a). Of these, *Capsicum annuum* annexin32/24 (ANN32/24) mediates Ca^{2+} influx in liposomes (Hofmann et al., 2000), while maize annexins ANN33 and ANN35 support a Ca^{2+}-permeable conductance in planar lipid bilayers (PLBs) (Laohavisit et al., 2009, 2010), and *Arabidopsis* ANN1 forms a K^+-permeable channel in PLB (Gorecka et al., 2007). More compelling evidence for annexins as ion transport pathways requires electrophysiological analysis of annexin mutants (Laohavisit et al., 2009; Konopka-Postupolska et al., 2011).

Expression and abundance of *Arabidopsis* ANN1 matches the occurrence of the $OH^{\bullet}$-activated PM Ca^{2+} conductance in the root epidermis and at the apex of root hairs (Clark et al., 2001, 2005; Dinneny et al., 2008). *ANN1* transcript abundance decreases by 24% as root epidermal cells mature (Dinneny et al., 2008), and the magnitude of the root epidermal PM $OH^{\bullet}$-activated conductance decreases by ~75% (Demidchik et al., 2003). ANN1 (one of eight annexins; Clark et al., 2001) can exist as an integral PM protein (Alexandersson et al., 2004; Lee et al., 1998; Santoni et al., 2004; Benschop et al., 2007; Marmagne et al., 2007). This makes ANN1 a prime candidate for the root epidermal PM $OH^{\bullet}$-activated conductance. We tested ANN1 function by applying electrophysiological analyses to the homozygous *ann1* knockout mutant and the complemented mutant *ann1/ANN1* (Lee et al., 2004). Recombinant ANN1 was used to reconstitute an $OH^{\bullet}$-activated Ca^{2+}-permeable conductance in PLBs. Cytosolic aequorin was deployed to assess the impact of *ann1* on $OH^{\bullet}$-activated $[Ca^{2+}]_{cyt}$ elevation. The results show that ANN1 supports the $OH^{\bullet}$-activated conductance of the root epidermal PM, contributes to regulation of $[Ca^{2+}]_{cyt}$, and plays a role in growth.

RESULTS

ann1 Lacks the PM $OH^{\bullet}$-Activated Conductance

Spheroplasts were released from the apices of young wild-type root hairs and the *ann1* homozygous single insert T-DNA knockout mutant (Lee et al., 2004). PM currents were obtained using the patch clamp whole-cell recording mode. In this, currents are generated as populations of channels open; negative current is influx of cations into the cytosol or efflux of anions. Ionic conditions were used previously to delineate $OH^{\bullet}$-activated currents in the wild type (Demidchik et al., 2003; Foreman et al., 2003). In controls, small inward and outward cation currents were observed at hyperpolarized and depolarized voltages, respectively, in both genotypes (Figures 1A and 1B). Mean values were not statistically significantly different between the wild type and *ann1* (see Supplemental Table 1 online; $n = 6$). Wild-type apical PM supported increased inward and outward cation currents in response to the generation of extracellular $OH^{\bullet}$ by 1 mM $CuCl_2$ and 1 mM ascorbic acid (Cu-Asc; Demidchik et al., 2003) (Figure 1A; see Supplemental Table 1 online; $n = 6$). The conductance would be competent in Ca^{2+} influx across the PM at root hair apical voltages (Felle et al., 1992). $OH^{\bullet}$-activated currents did not occur in *ann1* (Figure 1B; see Supplemental Table 1 online; $n = 6$). Root hair spheroplasts from the complemented *ann1/ANN1* line were too fragile for use in patch clamp recordings.

Protoplasts were obtained from mature cells of wild-type and *ann1* root epidermis. Control PM currents were not statistically significantly different between the wild type, *ann1*, and *ann1/ANN1* (Figures 1C to 1E; see Supplemental Table 1 online; $n = 6$). In controls, Cu or Asc alone had no significant effect on currents (see Supplemental Figures 1A to 1D online; $n = 3$), in agreement with previous studies (Demidchik et al., 2003; Foreman et al., 2003). Rectifying inward and outward currents were evoked when $OH^{\bullet}$ was generated by 1 mM Cu-Asc at the extracellular membrane face of the wild type (Figure 1C; see Supplemental Table 1 online; $n = 6$). Previously, removal of Ca^{2+} from the bath or K^+ from the pipette abolished the inward current and outward current, respectively (Demidchik et al., 2003). Here, when Ba^{2+} replaced Ca^{2+} in the bathing solution, an inward current was still observed in response to $OH^{\bullet}$ (see Supplemental Figure 1E online; $n = 3$), a response seen previously in root hair and epidermal PM (Demidchik et al., 2003; Foreman et al., 2003). As Ba^{2+} permeates Ca^{2+}-permeable channels but not K^+-inward rectifiers (Véry and Davies, 2000), these data confirm that an inward Ca^{2+} current was activated. At voltages more negative than the reversal potential for K^+ (E_K), it is feasible that K^+ made a small contribution to the inward current (see Supplemental Figure 1E online). Time dependency was more pronounced than reported previously for this cell type (Demidchik et al., 2003). The conductance would be competent in PM Ca^{2+} influx at normal root epidermal voltages (Demidchik et al., 2002). Currents were effectively abolished in *ann1* (even with increased observation

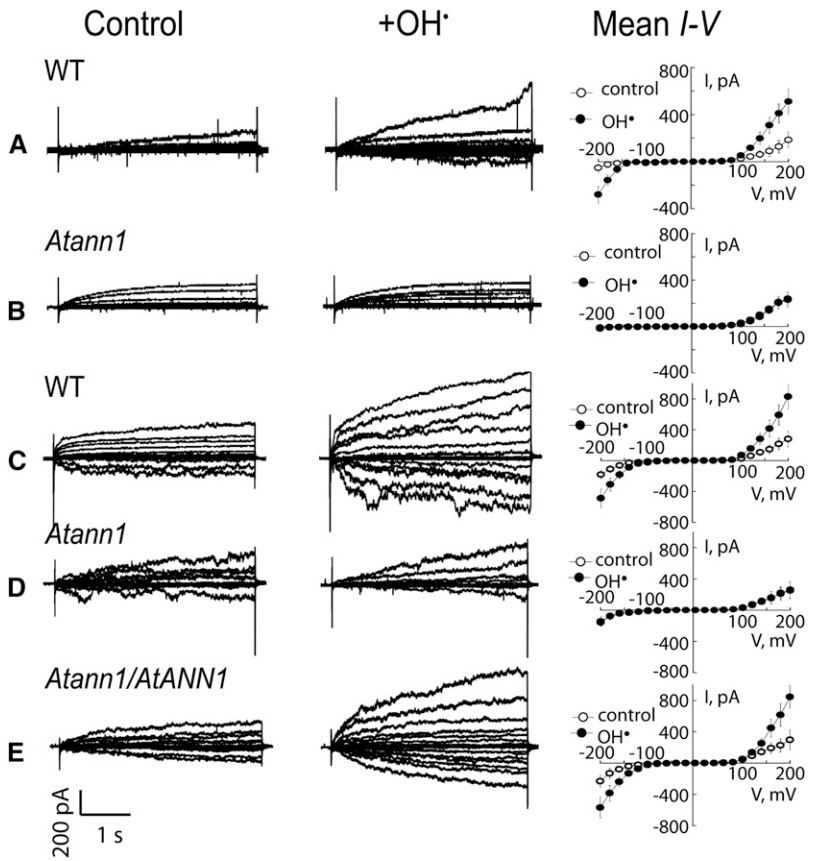

Figure 1. *ann1* Root Plasma Membrane Lacks the OH•-Activated Conductance.

(A) Whole-cell patch clamp recordings from wild-type (WT; Col-0) root hair apical spheroplast PM. Left: Control currents (*I*) elicited by step voltage (*V*) changes, from a representative spheroplast. Centre: *I* after exposure to extracellular OH• generated by 1 mM copper and 1 mM ascorbic acid (Cu-Asc). Holding potential was 0 mV. Right: mean ± SE. *I-V* relationships for control (open circles) and OH• exposure ($n = 6$). *I* below the *V* axis is cation entry into the spheroplast.

(B) As in **(A)** but for *ann1* ($n = 6$). Spheroplasts from the complemented mutant proved too fragile to patch clamp.

(C) As in **(A)** but for wild-type root epidermal protoplasts ($n = 6$).

(D) *ann1* root epidermal protoplasts ($n = 6$).

(E) Complemented mutant *ann1/ANN1* ($n = 6$). Bathing medium (mM): 20 $CaCl_2$, 0.1 KCl, 0.02 NaCl, and 5 MES-Tris, pH 5.6, adjusted to 270 mOsM with D-sorbitol. Pipette solution: 40 K-gluconate, 10 KCl, 0.4 $CaCl_2$, 1 mM BAPTA, and 2 MES-Tris, pH 7.2, adjusted to 270 mOsM with D-sorbitol.

time) but were restored in *ann1/ANN1* (Figures 1D and 1E; see Supplemental Table 1 online; $n = 6$). That *ann1/ANN1* currents were not greater than the wild type may indicate that ANN1 abundance or activity at the PM is tightly regulated in this cell type. Wild-type root hair apical PM and the root epidermal PM also contain a constitutive hyperpolarization-activated Ca^{2+} channel (HACC) that is involved in elongation (Véry and Davies, 2000; Demidchik et al., 2002). *ann1* spheroplasts still retained HACC activity, demonstrating that the HACC has a distinct molecular identity (Figure 2; $n = 3$). HACC-mediated current at −200 mV was approximately double that of the OH•-activated Ca^{2+} conductance. Accordingly, *ann1* root hairs still grew but were significantly shorter than the wild type on either low or replete nutrient medium. Growth was restored in *ann1/ANN1* (mean mature length, μm ± SD; low nutrient: wild type 383 ± 114, *ann1* 249 ± 117 [P = 0.001, Student's *t* test], *ann1/ANN1* 401 ± 129; replete medium: wild type 457 ± 128, *ann1* 404 ± 124 [P = 0.005], *ann1/ANN1* 435 ± 99; 100 root hairs per determination). These data are consistent with ANN1's operation in root hair elongation and the previous observation of short *ann1* primary roots (Clark et al., 2005).

ann1 Is Impaired in $[Ca^{2+}]_{cyt}$ Elevation

Extracellular OH• activate Ca^{2+} influx across the PM and cause elevation of $[Ca^{2+}]_{cyt}$ in root epidermis and root hairs (Demidchik et al., 2003; Foreman et al., 2003). As the PM OH•-activated Ca^{2+}-permeable conductance, ANN1 should be capable of elevating $[Ca^{2+}]_{cyt}$ and its loss of function would be expected to manifest as an impaired OH•-induced $[Ca^{2+}]_{cyt}$ increase. To test this, the *ann1* mutant was transformed to express cytosolic (apo)aequorin constitutively. When single excised roots were challenged with extracellular OH• (generated by Cu-Asc), a transient increase in $[Ca^{2+}]_{cyt}$ was observed in both genotypes,

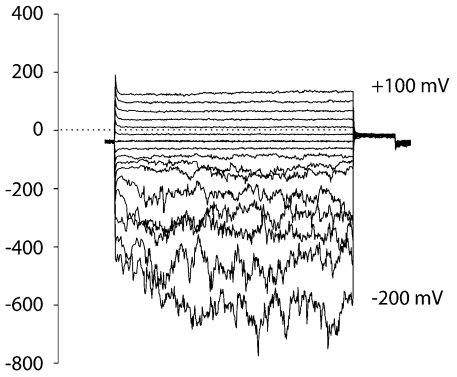

Figure 2. *ann1* Root Hair Apical PM Retains the Constitutive HACC Conductance.

Representative currents recorded in the whole-cell patch clamp configuration from an *ann1* root hair apical spheroplast PM showing the HACC conductance that is a characteristic of the root hair apex. No $OH^{\bullet}$ were used in this experiment, and Ba^{2+} replaced Ca^{2+} in the bathing medium. Current flowing below the time axis is cation entry into the protoplast. Bathing solution comprised 10 mM $BaCl_2$ and 2 mM MES-Tris, pH 6, adjusted to 275 mOsM with D-sorbitol. Pipette solution comprised 0.5 mM $CaCl_2$, 8.5 mM $Ca(OH)_2$, 2 mM MgATP, 0.5 mM Tris-ATP, 10 mM BAPTA (final free Ca^{2+}, 1 μM), and 15 mM HEPES-Tris, pH 7.3, adjusted to 275 mOsM with D-sorbitol.

but there was no significant difference between maximum $[Ca^{2+}]_{cyt}$ of the wild type (1.16 ± SE 0.03 μM, n = 3) and mutant (1.16 ± 0.06 μM, n = 3; P = 0.999, Student's t test). $[Ca^{2+}]_{cyt}$ returned to its basal level (~0.2 μM) after ~70 s in both genotypes. However, mathematical simulations suggest that cell-specific changes in $[Ca^{2+}]_{cyt}$ might not manifest at the whole-organ level (Dodd et al., 2006). Therefore, protoplasts were isolated from *ann1* root epidermis to test for a lesion in $[Ca^{2+}]_{cyt}$ regulation.

Buffer alone applied to root epidermal protoplasts elicited a transient $[Ca^{2+}]_{cyt}$ increase (touch response) of 0.82 ± SE 0.15 μM in the wild type (n = 4) and 0.58 ± 0.11 μM in *ann1* (Figure 3A; n = 4). Differences were not statistically different. Basal $[Ca^{2+}]_{cyt}$ was restored 10 s after the touch stimulus. The $[Ca^{2+}]_{cyt}$ increase evoked by extracellular $OH^{\bullet}$ was greater and more prolonged than the touch response in both genotypes. The maximum $OH^{\bullet}$-induced increase in $[Ca^{2+}]_{cyt}$ occurred after the maximum touch response (Figure 3A): 1.45 ± 0.058 μM in the wild type (at 4 s after stimulus, n = 4) and 1.12 ± 0.084 μM in *ann1* (at 5 s after stimulus, n = 4), a statistically significant 23% loss of signal in the mutant (P = 0.018). Basal $[Ca^{2+}]_{cyt}$ was regained more quickly in the mutant than the wild type, and when the area under the curve was calculated (36 to 75 s), $[Ca^{2+}]_{cyt}$ was statistically significantly lower in the mutant, consistent with a lesion in a Ca^{2+} influx pathway (wild type, 23.85 ± SE 0.9 μM; *ann1*, 17.08 ± 1.51 μM, P = 0.0084). That genotypic differences could be resolved at the population level of a single cell type rather than organ upholds the modeling predictions of Dodd et al. (2006). The lesion in the $[Ca^{2+}]_{cyt}$ response may be limited to the epidermis but does not appear to prevent propagation of the $[Ca^{2+}]_{cyt}$ response at the whole-root level.

To test if $[Ca^{2+}]_{cyt}$ increases came from PM Ca^{2+} influx, Gd^{3+} (300 μM) was applied prior to the stimulus to block influx channels. In Gd^{3+} controls, the touch response was 0.24 ± 0.083 μM in the wild type and 0.3 ± 0.91 μM in *ann1* (Figure 3B; n = 3), suggesting ANN1 does not participate in the touch response. Aligning time courses (Figure 3B) indicated that the touch response would be completed when the maximum response to $OH^{\bullet}$ occurred. Gd^{3+} delayed and weakened wild-type maximum response to $OH^{\bullet}$ (0.86 ± 0.085 μM, 11 s after application; n = 3; P = 0.0019), indicating block of PM Ca^{2+} influx. Wild-type maximum $[Ca^{2+}]_{cyt}$ response to $OH^{\bullet}$ under Gd^{3+} block was not significantly different to that of *ann1* without block (1.12 ± 0.084 μM), suggesting that Gd^{3+}-sensitive influx in the wild type was accounted for by ANN1 (Figure 3C). However, the presence of non-ANN1 transport routes was apparent in the response to $OH^{\bullet}$ of *ann1* under Gd^{3+} block (Figures 3B and 3C). There, the maximum $[Ca^{2+}]_{cyt}$ response was 0.71 ± 0.10 μM (12 s after application; n = 3), which was significantly lower than in *ann1* without Gd^{3+} (1.12 ± 0.084 μM; P = 0.025). While consequences of non-ANN1 transporters are evident in both genotypes, overall, the data confirm ANN1's acting in PM Ca^{2+} influx to mediate the $[Ca^{2+}]_{cyt}$ response to $OH^{\bullet}$ in a cell type known to support high levels of *ANN1* expression and harbor the $OH^{\bullet}$-activated PM cation conductance.

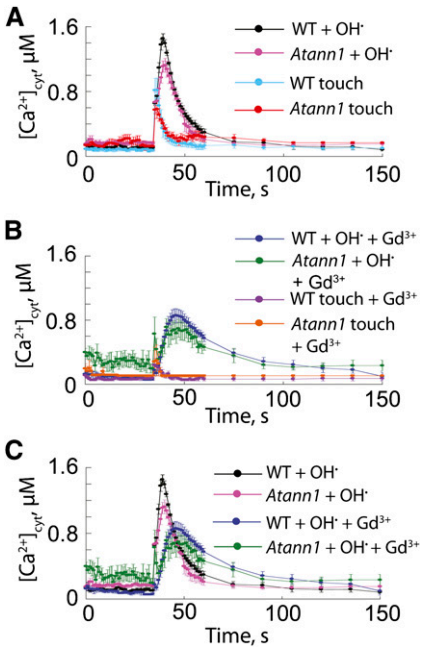

Figure 3. $OH^{\bullet}$-Activated $[Ca^{2+}]_{cyt}$ Increase in Root Epidermal Protoplasts Is Impaired in *ann1*.

(A) Root epidermal protoplast $[Ca^{2+}]_{cyt}$ was measured with cytosolic aequorin. Control touch response (buffer only at 35 s) was similar in the wild type (WT) and *ann1*. $OH^{\bullet}$ was generated by 0.5 mM Cu-Asc. Data are mean ± SE (n = 4). Buffer comprised 10 mM $CaCl_2$, 0.1 mM KCl, and 2 mM Tris/MES, pH 5.8, adjusted to 270 mOsM with D-sorbitol.

(B) As in **(A)** but protoplasts were incubated with 300 μM $GdCl_3$ for 30 min prior to $[Ca^{2+}]_{cyt}$ measurement (n = 3).

(C) Summary plot of experiments from **(A)** and **(B)** showing the effect of Gd^{3+} on $OH^{\bullet}$-induced $[Ca^{2+}]_{cyt}$ responses of wild-type and *ann1* protoplasts.

ANN1-Mediated K^+ Efflux Conductance Is Distinct to That of a Shaker-Like K^+ Channel

Root epidermal PM contains an $OH^{\bullet}$-activated Shaker-like K^+ efflux channel, GORK (for guard cell outward rectifying K^+ channel; Hosy et al., 2003), implicated in stress-induced cell death (Demidchik et al., 2010). Normal $OH^{\bullet}$-activated currents were observed in *gork* root epidermal PM, using the same conditions as for *ann1* (Figure 4; see Supplemental Table 1 online; $n = 6$). The $OH^{\bullet}$-activated K^+ efflux conductance seen in the wild type is most probably generated directly by ANN1; therefore, two distinct $OH^{\bullet}$-activated K^+ efflux pathways operate in root epidermis. As *gork* root growth is normal (Hosy et al., 2003), these data support a specific role for ANN1 in root elongation.

K^+ Efflux Is Impaired in Intact *ann1* Cells

The PM voltage of single, intact root epidermal cells in the elongation zone (measured with an impalement microelectrode) did not differ significantly between genotypes: the wild type ($-142 \pm$ SE 4 mV; $n = 7$), *ann1* (-141 ± 4 mV; $n = 7$), and *ann1/ANN1* (-134 ± 7 mV; $n = 5$). Respiratory inhibition with 0.1 mM NaCN and salicyl hydroxamic acid, to inhibit PM H^+-ATPase–mediated H^+ extrusion and reveal passive transport events (Leidi et al., 2010), evoked rapid membrane depolarization until the diffusion potential (E_D) was attained. E_D values were comparable between the wild type (-90 ± 4 mV; $n = 7$) and *ann1/ANN1* (-87 ± 4 mV; $n = 5$) but were more negative in the *ann1* mutant (-103 ± 3 mV; $n = 7$; $P = 0.05$). Extracellular $OH^{\bullet}$ evoked a small and transient hyperpolarization followed by a depolarization in the wild type (Figure 5A; $n = 3$) and *ann1/ANN1*. Hyperpolarization was not observed in *ann1* (Figure 5A; $n = 3$), and no differences were found in E_D values 5 min after $OH^{\bullet}$ treatment. Lack of arrest and reversal of the hyperpolarization in *ann1* is consistent with ANN1-mediated K^+ efflux (E_K was estimated to be approximately -156 mV) in response to extracellular $OH^{\bullet}$.

Loss of AtANN1 effectively abolished the net K^+ efflux from the root elongation zone in response to extracellular $OH^{\bullet}$ (Figures 5B and 5C; $n = 5$; no respiratory inhibitors). Maximum net K^+ efflux from *Atann1* was $-26 \pm$ SE 7 nmol·m^{-2}·s^{-1} ($n = 5$) compared with the wild type's -765 ± 149 nmol·m^{-2}·s^{-1} (Figure 5B; $n = 5$). Wild-type K^+ efflux was inhibited by 20 mM tetraethylammonium$^+$ (TEA), leaving a residual net flux with a maximum of -198 ± 12 nmol·m^{-2}·s^{-1} ($n = 5$) at 9.4 min after $OH^{\bullet}$ generation. Given that *Atann1* did not sustain a K^+ efflux response, this incomplete inhibition by TEA^+ in the wild type may represent incomplete penetration of this blocker. Complementation restored $OH^{\bullet}$-induced net K^+ efflux to 72% of the wild-type maximum ($n = 5$) but altered the time course of the response so that the peak flux occurred 6.3 min after the $OH^{\bullet}$ stimulus compared with the wild type at 16.8 min. Reasons for this are unclear at present. At the mature epidermis, kinetics and magnitude of net K^+ efflux elicited by $OH^{\bullet}$ from the wild type differed from that at the elongation zone (Figure 5D; $n = 5$). Maximum efflux was lower in the mature epidermis, a pattern observed previously (Demidchik et al., 2003). TEA^+ abolished the maximum component of the wild-type efflux response (wild type, -310 ± 46 nmol·m^{-2}·s^{-1} at 21.6 min; TEA^+, -55 ± 15 nmol·m^{-2}·s^{-1} at 21.6 min, $n = 5$), lowering it to the response shown by *ann1* (-87 ± 8 nmol·m^{-2}·s^{-1} at 21.6 min; Figure 5D; $n = 5$). Thus, the wild type's maximum component can be attributed to ANN1. Appreciable $OH^{\bullet}$-induced net K^+ efflux remained in *ann1*, but this was effectively abolished by TEA^+ (-6 ± 3 nmol·m^{-2}·s^{-1} at 21.6 min; Figure 5D; $n = 5$).

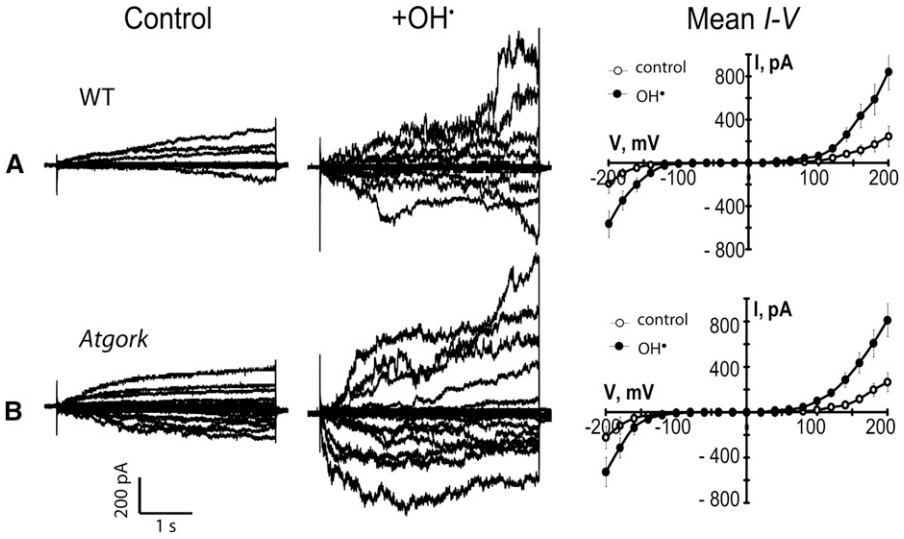

Figure 4. *Atgork* Root Epidermal PM Retains the $OH^{\bullet}$-Activated Conductance.

(A) Whole-cell recordings from wild-type (WT; Wassilewskija) root epidermal protoplasts. Left: Current traces under control conditions, elicited by step changes in voltage from a representative protoplast. Center: the same protoplast after exposure to extracellular $OH^{\bullet}$ generated by 1 mM Cu/Asc. Right: Mean $\pm$ SE current-voltage (*I-V*) relationships for control (open circles) conditions and $OH^{\bullet}$ exposure ($n = 6$). Recording conditions are as in Figure 1.
(B) As in **(A)** but with data gathered from *gork* ($n = 6$).

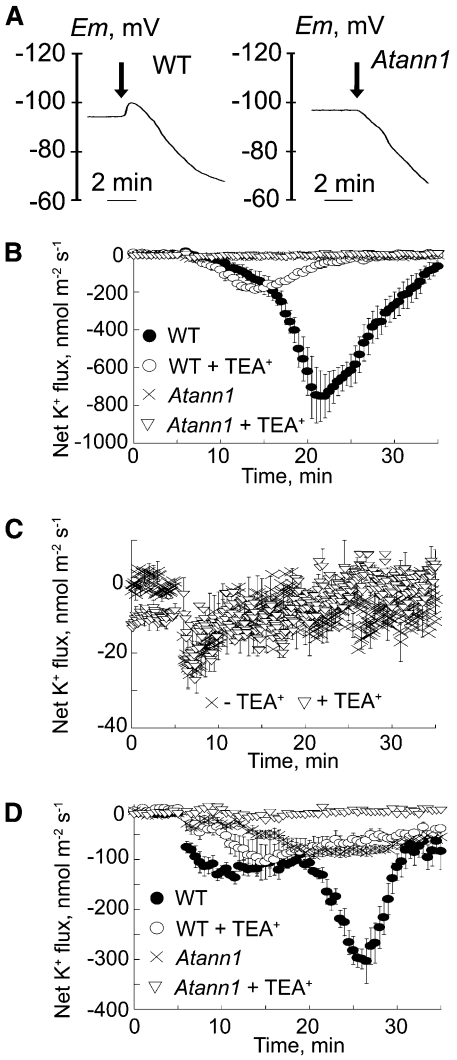

Figure 5. *ann1* Perturbs Diffusion Potentials and OH•-Activated Net K^+ Efflux of the Root Epidermis.

(A) Representative recordings of PM potential from wild-type (WT; Col-0) and *ann1* root elongation zone epidermis. Respiratory blockade was imposed by 0.1 mM NaCN-salicyl hydroxamic acid to reveal the diffusion potential (E_D). Extracellular OH• were generated by 0.5 mM Cu-Asc addition, as indicated by the arrow, resulting in a hyperpolarization in the wild type (left) but not *ann1* (right) followed by a similar depolarization in both lines (n = 3). Lack of arrest and reversal of the hyperpolarization in *ann1* is consistent with ANN1-mediated K^+ efflux (E_K was estimated to be approximately −156 mV) in response to extracellular OH•.

(B) Net K^+ efflux recorded from the wild-type (closed circles) and *ann1* (crosses) elongation zone epidermis using an extracellular vibrating K^+ electrode. Extracellular OH• were generated by 1 mM Cu-Asc addition at time = 0 min. TEA^+ was 20 mM (wild type, open circles; *Atann1*, open triangles). Negative values signify net efflux. Data are mean ± SE of five trials.

(C) *ann1* elongation zone response from **(B)** at greater resolution.

(D) As in **(B)** but values were recorded at the mature epidermis (n = 5). Recordings in the first 60 s after this addition were discarded to allow for establishment of diffusion gradients.

Purification of Recombinant ANN1

As a final test of the identity of the protein mediating the OH•-activated conductance, recombinant ANN1 was produced for incorporation in PLB. *ANN1* was cloned from the wild type (Columbia-0 [Col-0]), and the predicted protein sequence matched that reported in the National Center for Biotechnology Information database for ANN1 (NP 174810.1). *ANN1* was expressed in *Saccharomyces cerevisiae* (a null background for annexins; Creutz et al., 1992), and the protein was obtained by three cycles of Ca^{2+}-dependent binding to asolectin liposomes (Laohavisit et al., 2009). ANN1 (37 kD, matching the predicted mass) was detected in the supernatant by Coomassie blue staining and confirmed by immunoblotting using an anti-ANN1 peptide antibody (Figure 6). Silver staining revealed several contaminant protein bands, including a predominant band at ~60 kD, which was also found previously (Creutz et al., 1992) using *S. cerevisiae* to produce recombinant mammalian annexins. Analysis of the 60-kD yeast protein using matrix-assisted laser desorption/ionization (MALDI) peptide mass fingerprinting (searched against the yeast protein database) suggested three possible identities. These were Nuclear Signal Recognition1 (gi: 1323271), FK506-Sensitive Proline Rotamase3 (gi: 530998), and Survival Factor1 (gi: 6320553). ANN1 was not detected in preparations from an empty vector control.

Size exclusion chromatography was used to remove contaminants, an approach used previously for maize annexin purification (Laohavisit et al., 2009). The resultant fraction contained only ANN1, as shown by Coomassie blue staining, silver staining for 30 min, and immunoblotting (Figure 6). MALDI fingerprinting and electrospray ionization mass spectroscopy confirmed that the protein was ANN1; peptide fragments yielded 72% coverage. Overdeveloping the silver-stained gel (40 min) revealed very-low-level contaminants that were mostly also present in the buffer (Figure 6). To exclude the possibility that these contaminants were contributing to transport activity in PLB, the highly purified ANN1 preparation was immunoprecipitated for use in control experiments (Laohavisit et al., 2009, 2010).

ANN1 Reconstitutes an OH•-Activated Conductance

Recombinant ANN1 reconstituted a macroscopic OH•-activated Ca^{2+}-permeable influx conductance in PLB designed as a PM mimetic. These experiments were designed to resemble the patch clamp trials, so negative current is equivalent to cation influx to the cytosol. PLBs comprised 1-palmitoyl 2-oleoyl phosphatidylethanolamine, cholesterol, and 1-palmitoyl 2-oleoyl phosphatidylserine in a 5:3:2 ratio, respectively (Laohavisit et al., 2009). Phosphatidylserine binding is a conserved characteristic of annexin, while cholesterol stabilized the PLBs. With Ca^{2+} as the major cation, OH• in the *trans*-chamber (equivalent to patch clamping with OH• at the extracellular PM face) resulted in a cation-permeable conductance (after 35 ± 5 min) in six out of 10 attempts with ANN1 (3 μg) in the *cis*-chamber (Figure 7A; difference currents, produced by subtracting the control from test, are reported). OH• are membrane-impermeable hence lipid peroxidation most likely promoted conductance formation.

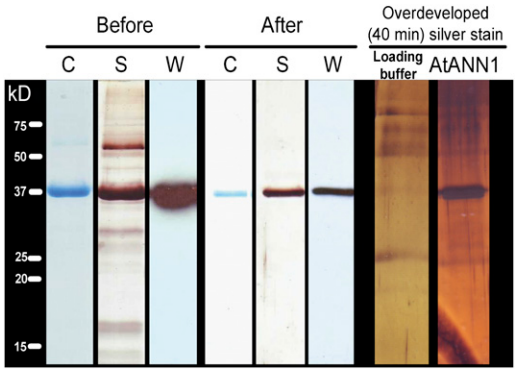

Figure 6. Purification of Recombinant ANN1.

ANN1 was expressed in *S. cerevisiae*, and the protein was purified by three cycles of Ca^{2+}-dependent binding to asolectin liposomes (Before) followed by size exclusion chromatography (After). The gel was either colloidal Coomassie blue stained (C), silver stained (S), or used to perform immunoblot analysis (W) to probe for ANN1 using anti-ANN1 peptide antibody. ANN1 is 37 kD. Overdeveloping the silver-stained gel revealed low-level contaminants that were also present in the buffer, including a predominant band at ~60 kD, which was also found when using *S. cerevisiae* to produce recombinant mammalian annexins. ANN1 was not detected in preparations from an empty vector control.

No conductance formed without $OH^{\bullet}$ (2-h observation; $n = 3$). Current was inwardly rectifying at hyperpolarized voltage (-14.5 ± 1 pA at -200 mV, $n = 6$; Figure 7A), consistent with Ca^{2+} influx from the *trans*- to *cis*-chamber and the inward Ca^{2+} current across the PM. Mean ± SE reversal voltage (E_{rev}) was 33 ± 4 mV ($n = 6$). The permeability ratio (Véry and Davies, 2000) $P_{Ca}:P_{Cl}$ was 34. The conductance was completely blocked by 50 μM Gd^{3+} (*trans*), confirming formation of a transport pathway by ANN1 (Figure 7A; $n = 6$). Thus, ANN1 reconstitutes an $OH^{\bullet}$-activated Ca^{2+}-permeable conductance that is sensitive to a blocker that inhibits $OH^{\bullet}$-induced PM Ca^{2+} conductance and $[Ca^{2+}]_{cyt}$ elevation in roots and protoplasts (Demidchik et al., 2003; Foreman et al., 2003).

With K^+ as the major cation, ANN1 supported an $OH^{\bullet}$-activated K^+ conductance in PLB. A K^+-permeable conductance was formed 53 ± 3 min after ANN1 addition (3 μg) under control conditions (four attempts out of six). $OH^{\bullet}$ in the *trans*-chamber caused transport activity in 26 ± 2 min (six out of eight attempts). Current was completely blocked by application of *trans* 50 mM TEA^+ (Figure 7B; difference currents reported, $n = 6$), consistent with block of At ANN1–mediated epidermal K^+ efflux. A $P_K:P_{Cl}$ of 53 was estimated for the $OH^{\bullet}$-activated K^+ conductance ($E_{rev} = -30 \pm 5$ mV, $n = 6$).

With both Ca^{2+} and K^+ gradients present to reflect patch clamp recording conditions and pH 6.0 in both chambers, a rectifying $OH^{\bullet}$-activated conductance was observed 39 ± 6 min after $OH^{\bullet}$ generation in nine out of 12 attempts (Figures 7C and 7D; difference currents reported). Even at lower voltages (± 20 mV), there was measurable current activation by $OH^{\bullet}$ (see Supplemental Figure 2 online). The E_{rev} was 4 ± 6 mV, close to the equilibrium potential (E) for H^+ (E_H 0 mV), suggesting that H^+ could be permeating rather than Ca^{2+}, K^+, or Cl^- (E_{Ca} +62 mV; E_K −137 mV; E_{Cl} −15 mV). However, setting E_H at −62 mV (with trans pH 7) had no significant effect on E_{rev} (5 ± 5 mV, $n = 5$; $P = 0.92$; Figure 7E). Using the $P_{Ca}:P_{Cl}$ and $P_K:P_{Cl}$ values obtained for the individual $OH^{\bullet}$-activated conductance, a $P_{Ca}:P_K$ of 0.6 was deduced (Véry and Davies, 2000) from the experiments with both K^+ and Ca^{2+} present and symmetrical pH. This is lower than obtained for animal annexins in PLB, but the effects of ROS on animal annexin selectivity are unknown. Gd^{3+} (50 μM) in the *trans*-compartment blocked all current generated by ANN1, regardless of the *trans* pH (Figures 7C to 7E; $n = 6$). In all control experiments, heat-inactivated preparation was ineffective ($n = 3$), as was immunoprecipitated ANN1 (see Supplemental Figure 3 online; $n = 4$). This demonstrates that even in PLB (imperfect mimics of PM), ANN1 forms an $OH^{\bullet}$-activated Ca^{2+}- and K^+-permeable pathway.

DISCUSSION

ANN1 function has been examined here from protein to cellular level, demonstrating its transport activity at the root epidermal PM, ability to perturb both $[Ca^{2+}]_{cyt}$ and K^+ efflux, plus its involvement in growth. Even in the highly simplified PLB environment (which did not perfectly mimic the physico-chemical complexity of the PM), ANN1 was capable of reconstituting a rectifying $OH^{\bullet}$-activated Ca^{2+}- and K^+-permeable conductance. This strongly resembled the rectifying $OH^{\bullet}$-activated Ca^{2+}- and K^+-permeable conductance of the wild-type root epidermal and root hair apical PM that was absent in the *ann1* mutant but restored by complementation. The longer lag time required for conductance formation in PLB compared with native membrane and cells might reflect the need for ANN1 to be lying in close proximity to the bilayer for $OH^{\bullet}$-activated transport events to occur or indicate that an interacting protein is required. Differences in ANN1 distribution between the PLB chamber and epidermal protoplast might also underpin the differences in the time dependency of the $OH^{\bullet}$-activated currents in PLB and patch clamp studies, respectively.

Recombinant ANN1 K^+ current was blocked by Gd^{3+} and TEA^+, which also block root epidermal $OH^{\bullet}$-activated K^+ efflux (Cuin and Shabala, 2007). TEA^+ brought $OH^{\bullet}$-activated net K^+ efflux from wild-type mature zone root epidermis to values supported by the *ann1* mutant, delineating the operation of ANN1 in intact cells. Moreover, $OH^{\bullet}$-activated net K^+ efflux was lost completely from the elongation zone epidermis of *ann1*. The function of this $OH^{\bullet}$-activated net K^+ efflux is at present unknown, but it could perhaps be involved in regulating membrane voltage. Results now point to two $OH^{\bullet}$-activated net K^+ efflux pathways being present in the root epidermis: ANN1 and the previously characterized *Arabidopsis* GORK (Demidchik et al., 2010). The ANN1-mediated $OH^{\bullet}$-activated K^+ efflux conductance was recorded in conditions that would suppress the Shaker-like GORK (low external K^+), suggesting that external K^+ may influence the operation of the two efflux pathways in vivo. For both, it can readily be envisaged that sustained production of $OH^{\bullet}$ could lead to their participation in K^+ loss leading to cell death (Demidchik et al., 2010).

Annexins have long been held to be a part of the plant cell's growth machinery, being abundant at polar growth points and being able to stimulate exocytosis (Carroll et al., 1998; reviewed

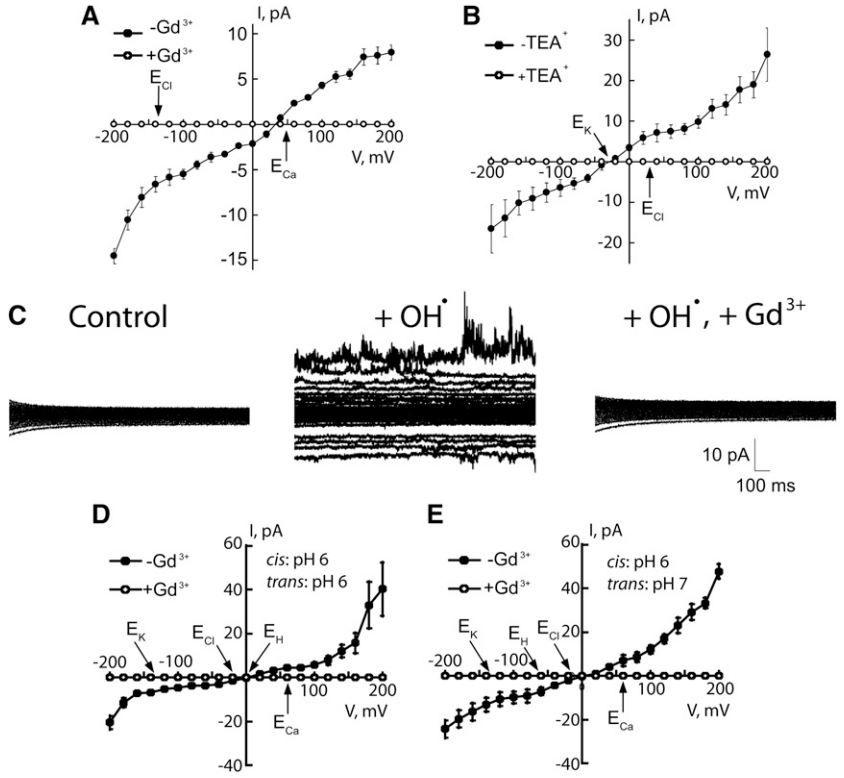

Figure 7. OH•-Activated Conductance Is Reconstituted by ANN1 in PLB.

(A) OH•-activated conductance mean ± SE. *I-V* with Ca^{2+} as the major cation: *cis*-chamber (mM) 1 Ca^{2+}, pH 6, ANN1 (3 μg); *trans* 200 Ca^{2+}, 1 Cu-Asc, pH 6. Positive *I* is positive charge movement from *cis* to *trans*. Current was blocked by 50 μM Gd^{3+} *trans* (open symbols; $n = 3$).

(B) OH•-activated conductance *I-V* with K^+ as the charge carrier: *cis*-chamber (mM) 200 KCl, pH 6, ANN1 (3 μg); *trans* 50 KCl, 1 Cu-Asc, pH 6.0 ($n = 4$). Current was blocked by *trans* 50 mM TEA^+ (open symbols; $n = 3$).

(C) Representative traces from one of six experiments with *cis* (mM) 200 K^+, 1 $CaCl_2$, and *trans* 1 K^+, 200 $CaCl_2$ both pH 6. Left: ANN1 (3 μg) in the *cis*-chamber; *V* was changed in 20-mV steps. Middle: OH• (1 Cu-Asc) in *trans* evoked inward and outward currents. Right: Block by 50 μM Gd^{3+} *trans*.

(D) I-V relationships for the OH•-activated conductance of **(C)**, $n = 5$ and Gd^{3+} block (open symbols; $n = 6$). Equilibria are indicated. Expanded current traces are shown in Supplemental Figure 2 online.

(E) OH•-activated conductance *I-V* with *cis*, pH 6, *trans*, pH 7.0, to change E_H. All other conditions are as in **(C)**; $n = 4$ without *trans* Gd^{3+}; $n = 6$ with 50 μM Gd^{3+}.

in Laohavisit and Davies, 2011a; Konopka-Postupolska et al., 2011). The ligon mutant of cotton (*Gossypium hirsutum*) is impaired in fiber elongation, and proteomic analysis revealed significant downregulation of five annexin isoforms when compared with the wild type, consistent with roles for annexins in growth (Zhao et al., 2010). ANN1's OH•-activated Ca^{2+} transport activity in PLB was consistent with a capacity for PM Ca^{2+} influx that could stimulate exocytosis. Accordingly, the Ca^{2+} transport lesion in *ann1* manifested in a significant impairment in epidermal cell PM-mediated OH•-activated $[Ca^{2+}]_{cyt}$ elevation. ANN1 supported 23% of the peak $[Ca^{2+}]_{cyt}$ response even though it is only one of over 20 possible channels in this cell type (Dinneny et al., 2008). Block of ANN1 by Gd^{3+} in PLB is consistent with Gd^{3+} inhibition of the wild type's OH•-stimulated $[Ca^{2+}]_{cyt}$ elevation in this and our previous study on root hairs (Foreman et al., 2003). Ca^{2+} influx at the root hair apex and elongation zone of the main root (where ANN1 is localized; Clark et al., 2001, 2005; Dinneny et al., 2008) is involved in growth and can be regulated by extracellular OH• (Foreman et al., 2003). ANN1 activation by OH• at acidic pH is consistent with its contributing to Ca^{2+} influx in root hair elongation, in which extracellular ROS are sourced by the RBOHC NADPH oxidase (Foreman et al., 2003) and apical cytosolic acidification oscillates (Monshausen et al., 2007). The short root and root hair phenotype of the *ann1* mutant can thus be attributed to the absence of a PM OH•-activated Ca^{2+} influx conductance mediated by ANN1. That root and root hair growth could still advance highlights the importance of other root PM Ca^{2+} channels, such as the HACC, the molecular identity of which now need to be resolved. Additionally, the question now arises of whether annexins function as Ca^{2+} influx transporters in other tip-growing cells in which growth is linked to NADPH oxidase activity, such as pollen tubes and fungal hyphae (Cano-Domínguez et al., 2008; Liu et al., 2009).

Ca^{2+} influx mediated by ANN1 may also help explain the drought and salt sensitivity of the *ann1* mutant (Konopka-Postupolska et al., 2009; Huh et al., 2010), particularly as plant

annexins have been proposed to act as sensors of stress and stress-evoked ROS (Gorecka et al., 2007; Laohavisit et al., 2010; Laohavisit and Davies, 2011a). In roots of *Arabidopsis* under salt stress, preventing the formation of or scavenging $OH^{\bullet}$ compromises the stability of the newly made mRNAs encoding for the PM Na^+/H^+ exporter Salt Overly Sensitive1 (SOS1; Chung et al., 2008). The ultimate source of the salt-induced ROS necessary for SOS1 mRNA stability is the NADPH oxidase RBOHC (Chung et al., 2008). This is also the NADPH oxidase that sources the ROS for the $OH^{\bullet}$-activated calcium conductance involved in root cell elongation (Foreman et al., 2003), shown here to be mediated by ANN1. Further studies are now required to ascertain whether ANN1 is involved in events leading to stabilizing SOS1 mRNA.

Animal annexins produce complex effects on ion transport across bilayers in vitro (reviewed in Konopka-Postupolska et al., 2011). In this study, ANN1 formed a macroscopic conductance, and single channel events were only rarely observed. Reasons for this are unclear. ANN1 was found previously to form single channel events in nonoxidized asolectin PLBs (Gorecka et al., 2007), and maize annexins ANN33/35 formed a 17 pS Ca^{2+}-permeable channel in PLBs containing malondialdehyde (Laohavisit and Davies, 2011b). Plant Ca^{2+}-permeable cation channel $P_{Ca}:P_K$ values range from 0.14 for nonselective cation channels (Demidchik and Maathuis, 2007) to orders of magnitude greater for HACCs (e.g., 15 for *Arabidopsis* root hair HACC (Véry and Davies, 2000). ANN1's estimated $P_{Ca}:P_K$ (0.6) is of similar magnitude to the conductance formed by maize ANN33/ANN35 in PLB (0.36; Laohavisit et al., 2009). Such values are lower than determined for animal annexins in PLB, albeit in nonoxidized conditions (e.g., 4.34 for annexin A5; Burger et al., 1994; Liemann et al., 1996) and indicate that residues other than those of the salt bridges may affect transport activity. PLBs and patch clamping are highly reductionist systems, and the permeability of ANN1 in vivo may well differ from values found here. The molecular identities of ROS-regulated Ca^{2+}-permeable channels in plants have remained obscure, despite their manifest significance in growth, adaptation, and defense (Dodd et al., 2010). The Ca^{2+}-permeable Stelar K^+ Outward K^+ Rectifier PM channel (Gaymard et al., 1998) has been shown to be activated by hydrogen peroxide in a heterologous expression system (Garcia-Mata et al., 2010), but the effects of ROS on its Ca^{2+} permeation, ability to affect $[Ca^{2+}]_{cyt}$, and where it lies in relation to NADPH oxidase activity are unknown. Maize ANN33/ANN35 have previously been shown to form a hyperpolarization-activated macroscopic Ca^{2+} conductance in PLBs containing malondialdehyde (to mimic peroxidized PM; Laohavisit et al., 2010). A greater mechanistic understanding of how annexins form conductance pathways in membranes, particularly membranes subject to modification by ROS, is now required so that their contribution to Ca^{2+} signaling governed by ROS in development and adaptation (Mittler et al., 2011) can be better understood. With the demonstration that a Ca^{2+} influx pathway requires ANN1, annexins of crop plants (Laohavisit and Davies, 2011a) can now be addressed confidently as components of growth and signaling, alongside the more conventional CNGCs, glutamate receptor–like channels, and Ca^{2+}-permeable high-affinity K^+ transporters as Ca^{2+} influx routes (Qi et al., 2006; Dodd et al., 2010; Lan et al., 2010; Ma et al., 2010; Michard et al., 2011).

METHODS

Plant Culture

Arabidopsis thaliana Columbia (Col-0) and Wassilewskija were the wild-type parental lines for the *ann1* and *gork* homozygous insertional T-DNA lines, respectively (Hosy et al., 2003; Lee et al., 2004). The 35S-complemented *ANN1* mutant was generated and described previously (Lee et al., 2004). For patch clamp, luminometry, and vibrating microelectrode experiments, plants were grown on Murashige and Skoog medium (Duchefa Biochemie) with 1% (w/v) Suc and 0.3% (w/v) Phytagel (Sigma-Aldrich). For impalement recordings and growth determinations, growth was on replete medium comprising (in mM) 5 KNO_3, 5 $MgSO_4 \cdot 7H_2O$, 2 NaCl, 1 $CaCl_2 \cdot 2H_2O$, 1 $(NH_4)_2HPO_4$, plus 0.1 $g \cdot 1^{-1}$ myo-inositol, 1 $mg \cdot L^{-1}$ thiamine, 0.5 $mg \cdot L^{-1}$ nicotinic acid, 0.5 $mg \cdot L^{-1}$ pyridoxine, 25 μM KCl, 25 μM Fe-Na EDTA, 17 μM H_3BO_3, 10 μM $MnSO_4 \cdot H_2O$, 10 μM $ZnSO_4 \cdot 7H_2O$, 2.5 μM $CuSO_4 \cdot 5H_2O$, 1% (w/v) Suc, 5 mM MES/Tris, pH 5.7, and 2% (w/v) agar. Nutrient-poor medium was as described previously (Véry and Davies, 2000): 0.1 mM $CaCl_2$, 0.1 mM KCl, pH 5.7, and 2% (w/v) agar. Growth was for 4 to 10 d at 22°C in a 16-h day at 100 $\mu mol \cdot m^{-2} \cdot s^{-1}$ irradiance. Mature root hair lengths were determined at day 4.

Patch Clamp Electrophysiology

The protoplasting protocol was adapted from Demidchik et al. (2003). Spheroplasts were released from young root hair apices using laser ablation (Véry and Davies, 2000). Standard patch clamp procedures were applied (Véry and Davies, 2000). For studies on epidermal protoplasts and the effects of hydroxyl radicals on root hair spheroplasts, bathing solution comprised 20 mM $CaCl_2$, 0.1 mM KCl, 20 μM NaCl, and 5 mM MES-Tris, pH 5.6, adjusted to 270 mOsM with D-sorbitol. The pipette solution comprised 40 mM K-gluconate, 10 mM KCl, 0.4 mM $CaCl_2$, 1 mM bis (2-aminophenoxy)ethane-*N,N,N′,N′*-tetraacetic acid (BAPTA), and 2 mM MES-Tris, pH 7.2, adjusted to 270 mOsM with D-sorbitol. For trials on root hair spheroplast constitutive HACC, bathing solution comprised 10 mM $BaCl_2$ and 2 mM MES-Tris, pH 6, adjusted to 275 mOsM with D-sorbitol. Pipette solution comprised 0.5 mM $CaCl_2$, 8.5 mM $Ca(OH)_2$, 2 mM MgATP, 0.5 mM Tris-ATP, 10 mM BAPTA (final free Ca^{2+}, 1 μM), and 15 mM HEPES-Tris, pH 7.3, adjusted to 275 mOsM with D-sorbitol.

Impalement and Vibrating Microelectrode Recordings

Seedlings (6 to 10 d old) were bathed in (mM) 0.2 KCl, 0.1 $CaCl_2$, 14 MES, and 5 Tris, pH 5.7. Membrane potential was measured in elongation zone epidermis using a 1-mm outer diameter microelectrode. Diffusion potential was achieved by superfusing with 0.1 mM NaCN and 0.1 mM salicyl hydroxamic acid (Leidi et al., 2010). Net fluxes of K^+ were measured noninvasively using the MIFE technique (Cuin and Shabala, 2007) in (mM) 0.2 KCl, 0.1 $CaCl_2$, pH 5.6, and ±20 TEA-Cl. Apical root segments (8 to 10 mm) were equilibrated in bathing solution for 50 min. Recordings were made 2 to 3 mm (mature epidermis) or 120 μm (elongation zone) from the apex. To test for $OH^{\bullet}$-induced changes in net K^+ flux, $CuCl_2$ and ascorbic acid were added simultaneously in bathing solution (1 mM final concentration). Recordings up to 60 s after this addition were discarded to allow for establishment of diffusion gradients. Significant differences in these and other trials were assessed with Student's *t* tests.

Protoplast $[Ca^{2+}]_{cyt}$ Determination

Col-0 and *ann1* were transformed using floral dip with *Agrobacterium tumefaciens* to express (apo)aequorin under a 35S promoter (Dodd et al., 2006). T3 generations were verified as *ann1*. Two independently generated lines per genotype yielding total photon counts in excess of 10^5 in rosette leaf Ca^{2+} discharge assays were used. Protoplasts were

incubated in aequorin buffer (mM: 10 $CaCl_2$, 0.1 KCl, and 2 Tris/MES, pH 5.8, adjusted to 270 mOsM with D-sorbitol) containing 10 μM coelentrazine (Lux Biotechnology) for 4 h in the dark. Protoplasts were washed with osmotically adjusted aequorin buffer without coelentrazine and resuspended in this (70 per μL). Suspension (100 μL) was placed into the well of a white 96-well plate (Greiner Bio-One), transferred to a plate-reading luminometer (FLUOstar OPTIMA; BMG Labtech), and left in the dark for 30 min. After recording baseline luminescence for 30 s, 50 μL of buffer (with or without $CuCl_2$) and 50 μL of buffer (with or without ascorbic acid) were injected (0.5 mM final concentration of $CuCl_2$/ascorbic acid). Luminescence was recorded every second for 30 s and then every 15 s for a further 2085 s. Discharge solution was then injected (final concentration: 10% [v/v] ethanol, 1 M $CaCl_2$), and luminescence was recorded for a further 120 s. Calibration to convert luminescent values to $[Ca^{2+}]_{cyt}$ was performed as described previously (Dodd et al., 2006).

Cloning of *ANN1*

RNA was isolated from whole seedlings using the RNeasy mini kit (Qiagen) and used to synthesize cDNA using the Superscript III first-strand synthesis system (Invitrogen). cDNA was purified and cleaned using QIAquick (Qiagen). The PCR reaction consisted of 100 ng cDNA, 250 nM primers, 250 μM deoxynucleotide triphosphate, 2 mM $MgCl_2$, 0.625 units of Biotaq DNA polymerase (Bioline), and 17 mM NH_4SO_4, pH 8.8. The primers were as follows: Ann 1-5-1, 5′-ATGGCGACTCTTAAGGTTTCTGATTC-3′; Ann 1-3-5, 5′-ACTATCATTAAGCATCATCTTCACCGAGAAGTGC-3′. The reaction was heated to 94°C for 2 min, followed by 30 cycles of denaturation (94°C, 20 s), annealing (50°C, 30 s), and extension (72°C, 2 min), followed by a final extension step (72°C, 10 min; iCycler, Bio-Rad). PCR products were analyzed by gel electrophoresis.

Heterologous Expression of *ANN1*

The pYES 2.1/V5-His Topo yeast expression vector (Invitrogen) was used for the expression of the *Arabidopsis ANN1* construct under the control of a Gal-inducible promoter. Fast-growing diploid *Saccharomyces cerevisiae* strain INVSc1 (genotype *Mat a, his 3D1, leu 2, trp1-289, ura3-52*; Invitrogen) was transformed with yeast expression vector (pYES 2.1/ V5-His Topo; Invitrogen) containing *ANN1*. Empty vector was used as a negative control. A single yeast colony was grown in liquid SC-U medium for 20 h at 30°C. Washed cells were resuspended in yeast extract/peptone YP medium to an OD_{600} of 0.18 and grown at 30°C, until an OD_{600} of 2 to 3 had been reached (18 h).

Purification of Recombinant ANN1

Cells were resuspended in extraction buffer (10 mM HEPES, 5 mM EGTA, 150 mM NaCl, and 0.01% [v/v] protease inhibitor cocktail [Sigma-Aldrich], pH 7.5) and disrupted by two cycles in an EmulsiFlex C5 homogenizer at 15,000 p.s.i. (Avestin). Debris were removed by centrifugation, the supernatant was incubated with DNase (5 μg mL^{-1}; Promega), RNase A (10 μg mL^{-1}; Roche Applied Science), and $MgCl_2$ (1 mM; 99.5% pure; Fisher Scientific) for 30 min at 180 rpm. Lysate was mixed with asolectin liposomes (200 mg soybean asolectin [Sigma-Aldrich] dissolved in (2:1) chloroform:methanol to give a final concentration of 13.3 mg/mL). $CaCl_2$ was added to a final concentration of 10 mM, and the mixture was incubated for 1 h. After centrifugation (30,000*g*, 30 min), the lipid pellet was resuspended in filter-sterilized wash buffer (50 mM HEPES, 150 mM NaCl, 10 mM $CaCl_2$, and 1 mM phenylmethanesulphonyl fluoride, pH 7.5). After a repeat centrifugation, the lipid pellet was resuspended in filter-sterilized wash buffer (50 mM HEPES and 10 mM $CaCl_2$, pH 7.5) and centrifuged (30,000 *g*, 30 min). The lipid pellet was resuspended in filter-sterilized elution buffer (50 mM HEPES and 10 mM EGTA, pH 7.5). After centrifugation (125,000*g*, 1 h), the final supernatant was mixed with asolectin liposomes, and the purification process was repeated twice. The buffer was exchanged to 100 mM NaCl and 50 mM K-phosphate buffer, pH 7.5, and samples were concentrated using a Vivaspin20 concentrator (molecular mass cutoff 10 kD; VivaScience). All steps were performed at 4°C. Samples were loaded onto a gel filtration column (Superose 12; GE Healthcare; equilibrated with 100 mM NaCl and 50 mM phosphate buffer, pH 7.5) attached to a fast performance liquid chromatography system. ANN1 was eluted at a flow rate of 0.4 mL/min. Fractions (1 mL) were tested for ANN1 by SDS-PAGE and immunoblotting. All proteins were exchanged into buffer (10 mM K-phosphate buffer, pH 7.4) prior to use. In immunoprecipitation studies, the ANN1 preparation was incubated for 30 min at room temperature with anti–At ANN1 peptide antibody (against NRYQDDHGEEIL, residues 204 to 215; Lee et al., 2004) in a 2:1 ratio (Laohavisit et al., 2009). Antibody alone was used as a control.

Gel Electrophoresis, Immunoblotting, and Protein Verification

Samples were subjected to SDS-PAGE as described previously (Laohavisit et al., 2009). In silver staining, gels were fixed overnight to enhance detection, washed twice for 20 min, and then stained for up to 40 min. For immunoblotting, membranes were incubated with primary antibody (1:5000 dilution) for 1 h, at room temperature, with shaking and then after washing incubated for 1 h with secondary antibody (1:5000 peroxidase-linked anti-rabbit IgG; Invitrogen). Proteins were visualized using enhanced chemiluminesence (ECL-plus; GE Healthcare). Mass spectrometry was used to determine protein identity. Samples were prepared for in-gel digestion as described previously (Laohavisit et al., 2009) and analyzed by MALDI peptide mass fingerprinting and electrospray ionization mass spectroscopy. Identifications were based on multiple peptide matches.

PLBs

Lipids (25 mg mL^{-1}; Avanti Polar Lipids) were used to form a bilayer (1-palmitoyl 2-oleoyl phosphatidylethanolamine:cholesterol:1-palmitoyl 2-oleoyl phosphatidylserine) in a 5:3:2 ratio, respectively, across a 200-μm diameter aperture at room temperature (20 to 24°C) (Laohavisit et al., 2009, 2010). In Ca^{2+}-permeability experiments, *cis*- and *trans*-chambers contained 0.5 mL 10 mM MES/*bis* Tris propane (BTP) and 1 mM $CaCl_2$, pH 6.0, and 2 mL 10 mM MES/BTP and 200 mM $CaCl_2$, pH 6.0, respectively. In K^+-permeability experiments, the *cis*-chamber comprised 200 mM KCl and 10 mM MES/BTP, pH 6.0, and the *trans* comprised 50 mM KCl and 10 mM MES/BTP, pH 6. In combined experiments, *cis* was 1 mM $CaCl_2$, 200 mM KCl, pH 6; *trans* was 200 mM $CaCl_2$, 1 mM KCl, pH 6.0 or 7. Annexin (3 μg) protein was added to the *cis*-chamber. The bilayer was held at −150 mV (*cis* negative) to aid insertion. Hydroxyl radicals were generated by adding 1 mM Cu-Asc to the *trans*-chamber. Conductance was monitored for annexin activity for up to 2 h. $GdCl_3$ or TEA-Cl were also added to *trans*. Results were from at least three separate protein preparations.

Accession Numbers

Sequence data from this article can be found in the EMBL/GenBank/National Center for Biotechnology Information RefSeq data library under accession number NP174810.1 for ANN1 (At1g35720; gb:AF083913).

Supplemental Data

The following materials are available in the online version of this article.

Supplemental Figure 1. Copper or Ascorbate Alone Do Not Elicit Plasma Membrane Currents; Copper and Ascorbate Together Elicit a Barium-Permeable Inward Conductance.

Supplemental Figure 2. Expanded Planar Lipid Bilayer Traces.

Supplemental Figure 3. Immunoprecipitated At ANN1 Does Not Support a Conductance in Planar Lipid Bilayers.

Supplemental Table 1. Root Plasma Membrane Currents.

ACKNOWLEDGMENTS

We thank Carlos Hotta, Thomas Martin, Anthony Miller, Yingzhen Yang, and Julian Schroeder for advice and Len Packman for peptide analyses. This work was supported by the University of Cambridge, the Biotechnology and Biological Science Research Council, the Royal Society, the Fulbright Foundation, and the Australian Research Council.

AUTHOR CONTRIBUTIONS

All authors contributed to research design and commented on the article. A.L., Z.S., L.R., A.-A.V., T.A.C., J.C.M., N.M., and K.M.C. performed the research and analyzed the data. J.M.D. wrote the article.

Received March 6, 2012; revised March 6, 2012; accepted March 21, 2012; published April 20, 2012.

REFERENCES

Alexandersson, E., Saalbach, G., Larsson, C., and Kjellbom, P. (2004). *Arabidopsis* plasma membrane proteomics identifies components of transport, signal transduction and membrane trafficking. Plant Cell Physiol. **45:** 1543–1556.

Balasubramanian, K., Bevers, E.M., Willems, G.M., and Schroit, A.J. (2001). Binding of annexin V to membrane products of lipid peroxidation. Biochemistry **40:** 8672–8676.

Benschop, J.J., Mohammed, S., O'Flaherty, M., Heck, A.J.R., Slijper, M., and Menke, F.L.H. (2007). Quantitative phosphoproteomics of early elicitor signaling in *Arabidopsis.* Mol. Cell. Proteomics **6:** 1198–1214.

Burger, A., Voges, D., Demange, P., Perez, C.R., Huber, R., and Berendes, R. (1994). Structural and electrophysiological analysis of annexin V mutants. Mutagenesis of human annexin V, an in vitro voltage-gated calcium channel, provides information about the structural features of the ion pathway, the voltage sensor and the ion selectivity filter. J. Mol. Biol. **237:** 479–499.

Cano-Domínguez, N., Alvarez-Delfin, K., Hansberg, W., and Aguirre, J. (2008). NADPH oxidases NOX-1 and NOX-2 require the regulatory subunit NOR-1 to control cell differentiation and growth in *Neurospora crassa*. Eukaryot. Cell **7:** 1352–1361.

Carroll, A.D., Moyen, C., Van Kesteren, P., Tooke, F., Battey, N.H., and Brownlee, C. (1998). Ca^{2+}, annexins, and GTP modulate exocytosis from maize root cap protoplasts. Plant Cell **10:** 1267–1276.

Chung, J.S., Zhu, J.K., Bressan, R.A., Hasegawa, P.M., and Shi, H. (2008). Reactive oxygen species mediate Na^+-induced *SOS1* mRNA stability in *Arabidopsis*. Plant J. **53:** 554–565.

Clark, G.B., Cantero-Garcia, A., Butterfield, T., Dauwalder, M., and Roux, S.J. (2005). Secretion as a key component of gravitropic growth: Implications for annexin involvement in differential growth. Gravit. Space Biol. Bull. **18:** 113–114.

Clark, G.B., Sessions, A., Eastburn, D.J., and Roux, S.J. (2001). Differential expression of members of the annexin multigene family in Arabidopsis. Plant Physiol. **126:** 1072–1084.

Creutz, C.E., Kambouris, N.G., Snyder, S.L., Hamman, H.C., Nelson, M.R., Liu, W., and Rock, P. (1992). Effects of the expression of mammalian annexins in yeast secretory mutants. J. Cell Sci. **103:** 1177–1192.

Cuin, T.A., and Shabala, S. (2007). Compatible solutes reduce ROS-induced potassium efflux in *Arabidopsis* roots. Plant Cell Environ. **30:** 875–885.

Demidchik, V., Bowen, H.C., Maathuis, F.J.M., Shabala, S.N., Tester, M.A., White, P.J., and Davies, J.M. (2002). *Arabidopsis thaliana* root non-selective cation channels mediate calcium uptake and are involved in growth. Plant J. **32:** 799–808.

Demidchik, V., Cuin, T.A., Svistunenko, D., Smith, S.J., Miller, A.J., Shabala, S., Sokolik, A., and Yurin, V. (2010). *Arabidopsis* root K^+-efflux conductance activated by hydroxyl radicals: Single-channel properties, genetic basis and involvement in stress-induced cell death. J. Cell Sci. **123:** 1468–1479.

Demidchik, V., and Maathuis, F.J.M. (2007). Physiological roles of nonselective cation channels in plants: From salt stress to signalling and development. New Phytol. **175:** 387–404.

Demidchik, V., Shabala, S.N., Coutts, K.B., Tester, M.A., and Davies, J.M. (2003). Free oxygen radicals regulate plasma membrane Ca^{2+}- and K^+-permeable channels in plant root cells. J. Cell Sci. **116:** 81–88.

Dinneny, J.R., Long, T.A., Wang, J.Y., Jung, J.W., Mace, D., Pointer, S., Barron, C., Brady, S.M., Schiefelbein, J., and Benfey, P.N. (2008). Cell identity mediates the response of *Arabidopsis* roots to abiotic stress. Science **320:** 942–945.

Dodd, A.N., Kudla, J., and Sanders, D. (2010). The language of calcium signaling. Annu. Rev. Plant Biol. **61:** 593–620.

Dodd, A.N., Kyed Jakobsen, M., Baker, A.J., Telzerow, A., Hou, S.W., Laplaze, L., Barrot, L., Poethig, R.S., Haseloff, J.P., and Webb, A.A.R. (2006). Time of day modulates Ca^{2+} signals in *Arabidopsis*. Plant J. **48:** 962–973.

Felle, H.H., Tretyn, A., and Wagner, G. (1992). The role of plasma membrane Ca^{2+}-ATPase in Ca^{2+} homeostasis in *Sinapsis alba* root hairs. Planta **188:** 306–313.

Foreman, J., Demidchik, V., Bothwell, J.H., Mylona, P., Miedema, H., Torres, M.A., Linstead, P., Costa, S., Brownlee, C., Jones, J.D., Davies, J.M., and Dolan, L. (2003). Reactive oxygen species produced by NADPH oxidase regulate plant cell growth. Nature **422:** 442–446.

Garcia-Mata, C., Wang, J., Gajdanowicz, P., Gonzalez, W., Hills, A., Donald, N., Riedelsberger, J., Amtmann, A., Dreyer, I., and Blatt, M.R. (2010). A minimal cysteine motif required to activate the SKOR K^+ channel of *Arabidopsis* by the reactive oxygen species H_2O_2. J. Biol. Chem. **285:** 29286–29294.

Gaymard, F., Pilot, G., Lacombe, B., Bouchez, D., Bruneau, D., Boucherez, J., Michaux-Ferrière, N., Thibaud, J.B., and Sentenac, H. (1998). Identification and disruption of a plant shaker-like outward channel involved in K^+ release into the xylem sap. Cell **94:** 647–655.

Gorecka, K.M., Thouverey, C., Buchet, R., and Pikula, S. (2007). Potential role of annexin AnnAt1 from *Arabidopsis thaliana* in pH-mediated cellular response to environmental stimuli. Plant Cell Physiol. **48:** 792–803.

Hofmann, A., Proust, J., Dorowski, A., Schantz, R., and Huber, R. (2000). Annexin 24 from *Capsicum annuum*. X-ray structure and biochemical characterization. J. Biol. Chem. **275:** 8072–8082.

Hosy, E., et al. (2003). The *Arabidopsis* outward K^+ channel GORK is involved in regulation of stomatal movements and plant transpiration. Proc. Natl. Acad. Sci. USA **100:** 5549–5554.

Huh, S.M., Noh, E.K., Kim, H.G., Jeon, B.W., Bae, K., Hu, H.C., Kwak, J.M., and Park, O.K. (2010). Arabidopsis annexins AnnAt1 and AnnAt4 interact with each other and regulate drought and salt stress responses. Plant Cell Physiol. **51:** 1499–1514.

Konopka-Postupolska, D., Clark, G., Goch, G., Debski, J., Floras, K., Cantero, A., Fijolek, B., Roux, S., and Hennig, J. (2009). The

role of annexin 1 in drought stress in *Arabidopsis*. Plant Physiol. **150:** 1394–1410.

Konopka-Postupolska, D., Clark, G., and Hofmann, A. (2011). Structure, function and membrane interactions of plant annexins: An update. Plant Sci. **181:** 230–241.

Kourie, J.I., and Wood, H.B. (2000). Biophysical and molecular properties of annexin-formed channels. Prog. Biophys. Mol. Biol. **73:** 91–134.

Kubista, H., Hawkins, T.E., Patel, D.R., Haigler, H.T., and Moss, S.E. (1999). Annexin 5 mediates a peroxide-induced $Ca^{(2+)}$ influx in B cells. Curr. Biol. **9:** 1403–1406.

Kwak, J.M., Mori, I.C., Pei, Z.M., Leonhardt, N., Torres, M.A., Dangl, J.L., Bloom, R.E., Bodde, S., Jones, J.D.G., and Schroeder, J.I. (2003). NADPH oxidase *AtrbohD* and *AtrbohF* genes function in ROS-dependent ABA signalling in *Arabidopsis*. EMBO J. **22:** 2623–2633.

Lan, W.Z., Wang, W., Wang, S.M., Li, L.G., Buchanan, B.B., Lin, H.-X., Gao, J.-P., and Luan, S. (2010). A rice high-affinity potassium transporter (HKT) conceals a calcium-permeable cation channel. Proc. Natl. Acad. Sci. USA **107:** 7089–7094.

Laohavisit, A., and Davies, J.M. (2011a). Annexins. New Phytol. **189:** 40–53.

Laohavisit, A., and Davies, J.M. (2011b) Annexins. In Coding and Decoding of Calcium Signals in Plants, S. Luan, ed (Berlin, Heidelberg: Springer), pp. 111–128.

Laohavisit, A., Brown, A.T., Cicuta, P., and Davies, J.M. (2010). Annexins: Components of the calcium and reactive oxygen signaling network. Plant Physiol. **152:** 1824–1829.

Laohavisit, A., Mortimer, J.C., Demidchik, V., Coxon, K.M., Stancombe, M.A., Macpherson, N., Brownlee, C., Hofmann, A., Webb, A.A.R., Miedema, H., Battey, N.H., and Davies, J.M. (2009). *Zea mays* annexins modulate cytosolic free Ca^{2+} and generate a Ca^{2+}-permeable conductance. Plant Cell **21:** 479–493.

Lee, S., Lee, E.J., Yang, E.J., Lee, J.E., Park, A.R., Song, W.H., and Park, O.K. (2004). Proteomic identification of annexins, calcium-dependent membrane binding proteins that mediate osmotic stress and abscisic acid signal transduction in *Arabidopsis*. Plant Cell **16:** 1378–1391.

Leidi, E.O., Barragán, V., Rubio, L., El-Hamdaoui, A., Ruiz, M.T., Cubero, B., Fernández, J.A., Bressan, R.A., Hasegawa, P.M., Quintero, F.J., and Pardo, J.M. (2010). The AtNHX1 exchanger mediates potassium compartmentation in vacuoles of transgenic tomato. Plant J. **61:** 495–506.

Liemann, S., Benz, J., Burger, A., Voges, D., Hofmann, A., Huber, R., and Göttig, P. (1996). Structural and functional characterisation of the voltage sensor in the ion channel human annexin V. J. Mol. Biol. **258:** 555–561.

Liu, P., Li, R.L., Zhang, L., Wang, Q.L., Niehaus, K., Baluska, F., Samaj, J., and Lin, J.X. (2009). Lipid microdomain polarization is required for NADPH oxidase-dependent ROS signaling in *Picea meyeri* pollen tube tip growth. Plant J. **60:** 303–313.

Ma, W., Smigel, A., Walker, R.K., Moeder, W., Yoshioka, K., and Berkowitz, G.A. (2010). Leaf senescence signaling: The Ca2+-conducting Arabidopsis cyclic nucleotide gated channel2 acts through nitric oxide to repress senescence programming. Plant Physiol. **154:** 733–743.

Marmagne, A., Ferro, M., Meinnel, T., Bruley, C., Kuhn, L., Garin, J., Barbier-Brygoo, H., and Ephritikhine, G. (2007). A high content in lipid-modified peripheral proteins and integral receptor kinases features in the *Arabidopsis* plasma membrane proteome. Mol. Cell. Proteomics **6:** 1980–1996.

Michard, E., Lima, P.T., Borges, F., Silva, A.C., Portes, M.T., Carvalho, J.E., Gilliham, M., Liu, L.H., Obermeyer, G., and Feijó, J.A. (2011). Glutamate receptor-like genes form Ca^{2+} channels in pollen tubes and are regulated by pistil D-serine. Science **332:** 434–437.

Mittler, R., Vanderauwera, S., Suzuki, N., Miller, G., Tognetti, V.B., Vandepoele, K., Gollery, M., Shulaev, V., and Van Breusegem, F. (2011). ROS signaling: The new wave? Trends Plant Sci. **16:** 300–309.

Monshausen, G.B., Bibikova, T.N., Messerli, M.A., Shi, C., and Gilroy, S. (2007). Oscillations in extracellular pH and reactive oxygen species modulate tip growth of *Arabidopsis* root hairs. Proc. Natl. Acad. Sci. USA **104:** 20996–21001.

Morgan, R.O., Martin-Almedina, S., Garcia, M., Jhoncon-Kooyip, J., and Fernandez, M.P. (2006). Deciphering function and mechanism of calcium-binding proteins from their evolutionary imprints. Biochim. Biophys. Acta **1763:** 1238–1249.

Müller, K., Linkies, A., Vreeburg, R.A.M., Fry, S.C., Krieger-Liszkay, A., and Leubner-Metzger, G. (2009). *In vivo* cell wall loosening by hydroxyl radicals during cress seed germination and elongation growth. Plant Physiol. **150:** 1855–1865.

Qi, Z., Stephens, N.R., and Spalding, E.P. (2006). Calcium entry mediated by GLR3.3, an Arabidopsis glutamate receptor with a broad agonist profile. Plant Physiol. **142:** 963–971.

Renew, S., Heyno, E., Schopfer, P., and Liszkay, A. (2005). Sensitive detection and localization of hydroxyl radical production in cucumber roots and *Arabidopsis* seedlings by spin trapping electron paramagnetic resonance spectroscopy. Plant J. **44:** 342–347.

Santoni, V., et al. (1998). Use of a proteome strategy for tagging proteins present at the plasma membrane. Plant J. **16:** 633–641.

Schrickel, J.W., et al. (2007). Enhanced heterogeneity of myocardial conduction and severe cardiac electrical instability in annexin A7-deficient mice. Cardiovasc. Res. **76:** 257–268.

Véry, A.A., and Davies, J.M. (2000). Hyperpolarization-activated calcium channels at the tip of *Arabidopsis* root hairs. Proc. Natl. Acad. Sci. USA **97:** 9801–9806.

Watson, W.D., Srivastava, M., Leighton, X., Glasman, M., Faraday, M., Fossam, L.H., Pollard, H.B., and Verma, A. (2004). Annexin 7 mobilizes calcium from endoplasmic reticulum stores in brain. Biochim. Biophys. Acta **1742:** 151–160.

Zhao, P.-M., Wang, L.-L., Han, L.-B., Wang, J., Yao, Y., Wang, H.-Y., Du, X.-M., Luo, Y.-M., and Xia, G.-X. (2010). Proteomic identification of differentially expressed proteins in the ligon lintless mutant of upland cotton (*Gossypium hirsutum* L.). J. Proteome Res. **9:** 1076–1087.

Arabidopsis Annexin1 Mediates the Radical-Activated Plasma Membrane Ca^{2+}- and K^{+}-Permeable Conductance in Root Cells

Anuphon Laohavisit, Zhonglin Shang, Lourdes Rubio, Tracey A. Cuin, Anne-Aliénor Véry, Aihua Wang, Jennifer C. Mortimer, Neil Macpherson, Katy M. Coxon, Nicholas H. Battey, Colin Brownlee, Ohkmae K. Park, Hervé Sentenac, Sergey Shabala, Alex A.R. Webb and Julia M. Davies

Plant Cell; originally published online April 20, 2012;
DOI 10.1105/tpc.112.097881